Regenerated Synapses in Lamprey Spinal Cord Are Sparse and Small Even After Functional Recovery From Injury

Paul A. Oliphint,[1] Naila Alieva,[1] Andrea E. Foldes,[1] Eric D. Tytell,[2] Billy Y.-B. Lau,[1] Jenna S. Pariseau,[3] Avis H. Cohen,[2] and Jennifer R. Morgan[1]*

[1]Section of Molecular Cell and Developmental Biology; Institute for Cell and Molecular Biology, Institute for Neuroscience, University of Texas at Austin, Austin, Texas 78712

[2]Department of Biology, Program in Neuroscience and Cognitive Science, Institute for Systems Research, University of Maryland, College Park, Maryland 20742

[3]Biology Department, Bowdoin College, Brunswick, Maine 04011

ABSTRACT

Despite the potential importance that synapse regeneration plays in restoring neuronal function after spinal cord injury (SCI), even the most basic questions about the morphology of regenerated synapses remain unanswered. Therefore, we set out to gain a better understanding of central synapse regeneration by examining the number, distribution, molecular composition, and ultrastructure of regenerated synapses under conditions in which behavioral recovery from SCI was robust. To do so, we used the giant reticulospinal (RS) neurons of lamprey spinal cord because they readily regenerate, are easily identifiable, and contain large synapses that serve as a classic model for vertebrate excitatory neurotransmission. Using a combination of light and electron microscopy, we found that regenerated giant RS synapses regained the basic structures and presynaptic organization observed at control giant RS synapses at a time when behavioral recovery was nearly complete. However, several obvious differences remained. Most strikingly, regenerated giant RS axons produced very few synapses. In addition, presynaptic sites within regenerated axons were less complex, had fewer vesicles, and had smaller active zones than normal. In contrast, the densities of presynapses and docked vesicles were nearly restored to control values. Thus, robust functional recovery from SCI can occur even when the structures of regenerated synapses are sparse and small, suggesting that functional recovery is due to a more complex set of compensatory changes throughout the spinal network. J. Comp. Neurol. 518:2854–2872, 2010.

INDEXING TERMS: actin; active zone; axon; synaptic vesicle; ultrastructure

Spinal cord injury (SCI) in mammals often leads to a permanent impairment of movements and sensations due to a widespread loss of axons and synapses within the central nervous system (CNS). This loss of axons and synapses occurs when the proximal portions of damaged axons retract, or "die back," and the distal portions of damaged axons undergo Wällerian degeneration (Ramón y Cajal, 1991; Kerschensteiner et al., 2005). Subsequently, axon and synapse regeneration are limited, thereby contributing to the lack of functional recovery (Steward et al., 2003; Case and Tessier-Lavigne, 2005; Harel and Strittmatter, 2006; Maier and Schwab, 2006). As a result, a great deal of effort has been invested in identifying factors that prevent or that promote axon regeneration in order to develop strategies for restoring greater function to the injured spinal cord (Bradbury and McMahon, 2006; Yiu and He, 2006; Lu and Tuszynski, 2008; Ruff et al., 2008). However, function will not be restored unless regenerating or sprouting axons form

Grant sponsor: University of Texas-Austin; Grants: start-up funds and Science and Technology Acquistion and Retention (STARS) Award (to J.R.M.) and Undergraduate Research Fellowship (to A.E.F.); Grant sponsor: NIH; Grant number: RO1NSO5427102 (to A.H.C.).

*CORRESPONDENCE TO: Jennifer R. Morgan, Ph.D., Section of Molecular Cell and Developmental Biology, University of Texas at Austin, 2401 Speedway, Austin, TX 78712. E-mail: jmorgan@mail.utexas.edu

Received November 16, 2009; Revised January 15, 2010; Accepted February 24, 2010

DOI 10.1002/cne.22368

Published online March 23, 2010 in Wiley InterScience (www.interscience.wiley.com)

sufficient numbers of synapses with appropriate strengths onto suitable targets.

Despite its potential importance for restoring function after SCI, surprisingly little is known about synapse regeneration. Several studies have demonstrated that regenerating mammalian CNS axons are capable of forming synapses (Havton and Kellerth, 1987; Campos et al., 2008). In an invertebrate, the leech, and in several vertebrates, lampreys and opossums, regenerating CNS axons form synapses with the appropriate class of postsynaptic targets (Muller and Scott, 1979; Mackler and Selzer, 1987; Mladinic et al., 2009). However, in mammals, compensatory sprouting of spared axon collaterals, as well as formation of novel relay connections, potentially circumvents the need for extensive regeneration in the partially injured spinal cord (Weidner et al., 2001; Bareyre et al., 2004; Courtine et al., 2008; Steward et al., 2008; Blesch and Tuszynski8, 2009). Consequently, sprouting can complicate a rigorous analysis of true axon and synapse regeneration across the lesioned area (Steward et al., 2003). In addition, the small size of most vertebrate synapses and their existence within complex neural networks makes it difficult to identify and assay them to any large degree (Bareyre et al., 2004; Becker et al., 2004; Ballermann and Fouad, 2006). Therefore, some of the most basic questions about the structures and molecular features of regenerated synapses remain unanswered. Do regenerated axons make more synapses than normal to compensate for the damage-induced loss of axonal material, or do they make fewer synapses? Are regenerated synapses structurally and molecularly similar to normal synapses, or do they adopt a novel composition?

At present, these basic questions about CNS synapse regeneration are best answered by using the spinal cord of lampreys, which are basal extant vertebrates (Osorio and Retaux, 2008). In lampreys, spinal cord transection severs the entire population of descending neurons, particularly the reticulospinal (RS) neurons that initiate and modulate locomotion (Orlovsky et al., 1992; Deliagina et al., 2000; Fagerstedt et al., 2001; Dubuc et al., 2008). This includes a subset of giant RS neurons, the Müller and Mauthner cells, which have exceptionally large axons and synapses (Rovainen, 1979; Wickelgren et al., 1985). Within a few months after transection, lampreys regain coordinated swimming behaviors (Rovainen, 1976; Cohen et al., 1986; Ayers, 1989; Davis et al., 1993), implying that synapse function is restored to some extent somewhere within the locomotor network. During the recovery period, approximately half of the small and giant RS axons spontaneously regenerate across the scar (Rovainen, 1976; Selzer, 1978; Davis and McClellan, 1993). Due to their large size, the giant RS axons provide an easily identifiable compartment for examining regenerated CNS synapses (Wood and Cohen, 1981; Lurie et al., 1994). In addition to having regenerative capacity, the giant RS synapses are glutamatergic and share many other molecular and structural features in common with other model synapses (Pieribone et al., 1995; Photowala et al., 2005; Brodin and Shupliakov, 2006), lending relevance to higher vertebrates. Taken together, these combined features make lamprey giant RS neurons an ideal model in which to examine CNS synapse regeneration.

Some of the basic structural and functional characteristics of regenerated giant RS synapses have been described. Morphological studies revealed that regenerated giant RS synapses contain all of the key elements of chemical synapses, including a vesicle cluster, synaptic cleft, and postsynaptic dendrite (Wood and Cohen, 1979, 1981). In contrast, there is no evidence for regeneration of the electrical component of giant RS synapses, which is typically identified structurally by the presence of a gap junction and functionally by direct coupling (Wood and Cohen, 1981; Mackler and Selzer, 1987). Finally, regenerated giant RS axons selectively form synapses with the original class of postsynaptic targets while avoiding nontarget neurons, as determined by combined intracellular recordings and cell labeling (Mackler and Selzer, 1985, 1987). However, a broader, more quantitative evaluation of the number, axonal distribution, molecular composition, and ultrastructural features of an entire population of regenerated CNS synapses has yet to be reported in any vertebrate, including lampreys.

Here, we used a combination of light and electron microscopy to examine regenerated lamprey giant RS synapses under conditions of robust functional recovery. Surprisingly, regenerated giant RS axons produced very few synapses, compared with the number they normally have. Regenerated giant RS synapses were also simpler and smaller than control synapses of intact spinal cords. In contrast, other features of regenerated synapses, such as their axonal density, presynaptic organization, and docked vesicles, were at least partially restored. Taken together, these data indicate that regenerated axons need not produce normal synapse numbers and structures as a general requirement for functional recovery. Instead, recovery of effective behavior likely involves complex compensatory changes at diverse locales within the locomotor network.

MATERIALS AND METHODS

Spinal cord transection

Late larval stage lampreys (*Petromyzon marinus*; 10–14 cm) were acquired from Lamprey Services (Ludington, MI) or Acme Lamprey Company (Bowdoin, ME) and were housed at room temperature (RT; 22–25°C) in standard

10-gallon aquaria. Prior to surgery, lampreys were anesthetized with Finquel MS-222 (0.1 g/liter tank water; Argent Chemical Laboratories, Redmond, WA). After anesthesia was complete, spinal cord transections were performed as previously described (Jacobs et al., 1997). Briefly, each lamprey was placed on a sponge moistened with aerated lamprey Ringer's solution (in mM): 91 NaCl, 2.1 KCl, 2.6 $CaCl_2$, 1.8 $MgCl_2$, 4 glucose, 0.5 glutamine, 2 HEPES, pH 7.4. A dorsal incision was made at the level of the 5th gill through the musculature and fat tissue, in order to expose the spinal cord. Then the spinal cord was completely transected with a single horizontal cut by using fine iridectomy scissors. Transection was confirmed visually by examining the cut ends. The incision was closed with a single suture (Ethilon 6-0 black monofilament nylon; Johnson & Johnson, Langhorn, PA), and the lamprey was moved back to a holding tank for recovery. The transection was deemed successful if the lamprey exhibited paralysis below the lesion immediately upon awaking from anesthesia. For all experiments, the lampreys were allowed to recover for 10–12 weeks at RT (22–25°C), a condition in which segmental coordination of muscle activity and swimming spontaneously return to nearly normal levels (Fig. 1) (Ayers, 1989; Davis et al., 1993; Cohen et al., 1999).

Behavioral and kinematic analyses

For nine transected lampreys, swimming movements were scored twice per week by using an approach similar to the ones previously described (Ayers, 1989; Cooke and Parker, 2009). In the current study, a "movement score" of 0 indicates that the lamprey was paralyzed completely below the transection site and that it did not respond to a touch stimulus (a light pinch) to either the head or the tip of the tail. A score of 1 indicates that the lamprey responded with some tail movements, but that no forward swimming occurred. A score of 2 indicates that the lamprey exhibited brief, abnormal bouts of self-initiated swimming, which often included unusual start-stop behaviors, rapid head oscillations, and atypical body contractions. A score of 3 indicates that the lamprey exhibited more persistent bouts of swimming in which the undulations were more regular. However, at this stage, atypical body contractions were sometimes still apparent, and lampreys often had difficulty swimming in an upright position. A score of 4 indicates that the lampreys exhibited persistent bouts of continuous swimming, characterized by undulations that appeared normal. As an example, in Figure 1B–D, the lampreys at 1 week, 3 weeks, and 12 weeks post-transection received scores of 1, 2 (or 3), and 4, respectively.

Along with behavioral scoring, swimming kinematic parameters were also estimated for six uninjured control lampreys and six transected lampreys at 10–12 weeks post-transection. Swimming behaviors were recorded by using a Sony DCR-SR42 Handycam video camera. Between 13 and 25 swimming sequences were recorded for each lamprey, which contained more than 100 total tail beats for most animals. From the videos, midlines and kinematic parameters, including tail beat frequency, body wavelength, and wave speed, were estimated by using DigitizeFish software custom written and developed in Matlab 7.1 (Mathworks, Natick, MA). Body wavelength (λ) is equal to twice the distance between successive peaks of curvature along the body (see Fig. 1D). Details of the estimation algorithm are published elsewhere (Tytell and Lauder, 2004).

Spinal cord dissection

At the time of the experiments, uninjured control lampreys and transected lampreys were anesthetized in MS-222 (0.1 g/liter tank water), followed by dissection and excision of 3–4 cm of the rostral spinal cord. For transected lampreys, this typically included $\sim$1 cm of spinal cord proximal to the lesioned area and 2–3 cm of spinal cord distal to the lesioned area. Spinal cords were pinned ventral side up in a Sylgard-lined dish for easy access to the giant RS axons, submerged in oxygenated lamprey Ringer's solution, subjected to removal of the *meninx primativa*, and then microinjected or fixed as described below. In this study, 28 control lamprey spinal cords and 43 transected lamprey spinal cords (10–12 weeks post-transection) were used. All procedures were in compliance with the National Institutes of Health standards and were approved by the Institutional Animal Care and Use Committee at the University of Texas at Austin.

Axonal microinjections and horseradish peroxidase labeling

Giant RS axons of control lampreys and transected lampreys (at 10–12 weeks of recovery) were labeled by intra-axonal microinjection of horseradish peroxidase (HRP). To do so, giant RS axons were impaled at a position 1–2 mm proximal to the 5th gill region (i.e., the lesion site in transected spinal cords) with glass micropipettes (15–40 MΩ), which were preloaded with 4% HRP in lamprey internal solution (180 mM KCl; 10 mM HEPES, pH 7.4). The HRP was then injected into individual giant RS axons by delivery of small, repeated puffs of N_2 (10 ms; 0.3 Hz; 40 psi) by using a Toohey spritzer (Toohey, Fairfield, NJ). Because HRP cannot be visualized directly during the injection, fluorescent Texas Red (TxRd) dextran (0.1 mM in lamprey internal solution; 3 kDa, lysine fixable; Invitrogen, Carlsbad, CA) was co-injected along with HRP, allowing immediate assessment of the axon's identity and the relative amount of HRP being injected. Throughout the axonal injection, which typically lasted 10–30 minutes, the

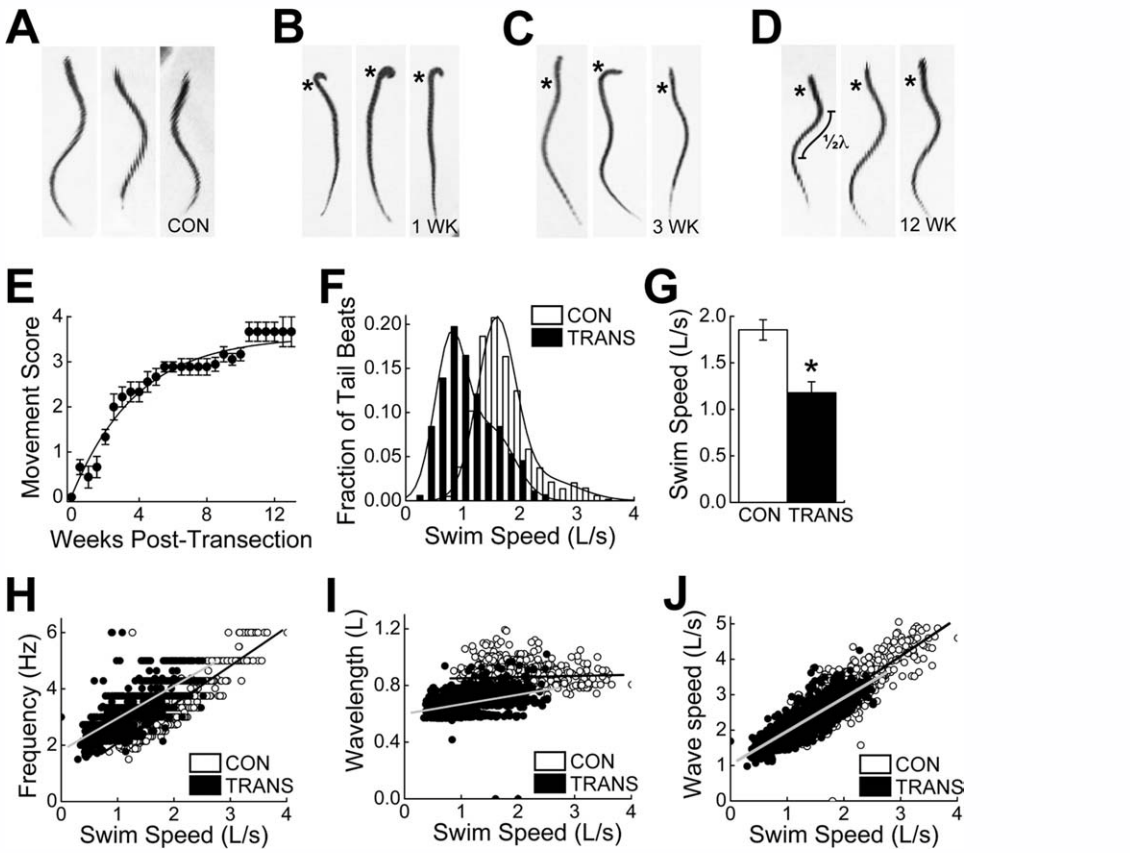

Figure 1. Recovery of swimming behavior after SCI in lampreys. **A–D**: Images of individual control (CON) lampreys (A) and spinal-transected (TRANS) lampreys after 1 week (B), 3 weeks (C), and 12 weeks (D) of recovery. Undulatory swimming movements are impaired at 1 and 3 weeks post-transection. However, more normal swimming returns by 12 weeks post-transection. Asterisks mark the transection site. In D, measurement of body wavelength (λ; see I) is indicated. **E**: Time course of behavioral recovery shows a nearly complete recovery of swimming movements. Data points represent the mean movement score ± SEM from nine spinal-transected lampreys (see Materials and Methods for details). Line represents the best fit of a hyperbolic function to the data points ($R^2 = 0.97$). **F–J**: Data comparing kinematics of swimming between control lampreys ($n = 6$) and spinal-transected lampreys after 10–12 weeks of recovery ($n = 6$). Although functional recovery is robust, some differences in swim speed (F,G), tail beat frequency (H), and body wavelength (I) persist. The normal relationship of body wave speed to swim speed was largely restored (J), if one accounts for the slower swimming in transected animals. In all panels, "L" stands for body length.

TxRd dextran was visualized periodically by using a Zeiss Axioskop 2FS compound microscope (10×, 0.3 NA objective; Zeiss Plan-NEOFLUAR; Chroma 546/12 nm BP filter). After injection, the HRP was initially allowed to diffuse for 1–3 hours. Then the HRP was developed by using a procedure that was slightly modified from previous studies (Yin and Selzer, 1983; Davis and McClellan, 1994). Specifically, the entire, unfixed spinal cord was reacted for 2–10 minutes with 0.075% hydrogen peroxide in Hanker-Yates solution (Sigma-Aldrich, St. Louis, MO), at which point the HRP activity generated a brown reaction product in labeled axons and their branches. In the first few experiments, spinal cords were fixed immediately after the development in 4% paraformaldehyde (PFA) in 0.1 M phosphate-buffered saline (PBS; pH 7.4). However, the HRP labeling of small axon branches and terminal axon tips was much better when we allowed the developed HRP to diffuse in unfixed spinal cords overnight (12–16 hours) at 4°C before fixation in PFA. Therefore, this approach was used in all subsequent experiments. Only axons in which HRP could be traced to the terminal axon tip were included in the analyses presented in Figure 2.

Imaging of HRP-labeled axons was performed on a Leica MZ16 fluorescence stereomicroscope (1.0×, 0.14 NA PlanApo lens; Leica Application Suite Version 2.8.0; Leica Microsystems, Bannockburn, IL). From these images, the percentage of HRP-labeled giant RS axons that regenerated across the lesion scar was estimated by dividing the total number of injected axons by the number whose terminal tips grew beyond the center of the lesion scar. The percentage of HRP-labeled axons that adopted a particular morphology (e.g., branching, rostral turning, termination, midline crossings) was also determined. Distances of axon regeneration were measured with Image J software (NIH) by tracing the axons' paths from the center of the lesion site to the distal axon tips.

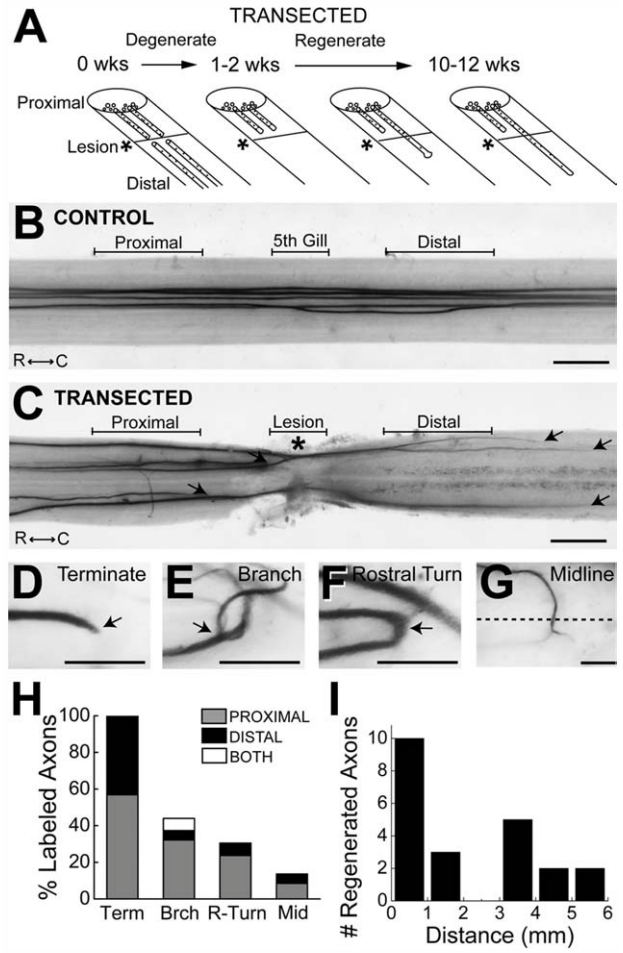

Figure 2. Giant RS axon regeneration. **A**: Diagram showing the time course of giant RS axon degeneration and regeneration after spinal cord transection, based on previous studies. **B,C**: Bright-field images of an unlesioned, control lamprey spinal cord (B) and a transected spinal cord after 10 weeks of recovery (C) in which five giant RS axons were microinjected with HRP. Note the straight, unbranching appearance of the control giant RS axons. In contrast, in transected spinal cords, giant RS axons terminated both proximal and distal to the lesion scar (arrows). Rostral (R) and caudal (C) orientations are indicated. Proximal, 5th gill/Lesion, and Distal designations indicate the regions in which giant RS synapses were examined in subsequent figures. Asterisk indicates the center of the lesion. **D–G**: High-magnification images of HRP-labeled giant RS axons at 10–12 weeks post transection. Many atypical structures were observed, including axon terminations (D), branches (E), rostral turns (F), and midline crossings (G). Arrows point to the structure of interest. Dashed line in G indicates the spinal cord midline. **H**: Graph showing the percentages of giant RS axons within transected spinal cords that exhibited termination (Term), branching (Brch), rostral turning (R-turn), and midline crossing (Mid). Whether the structures were observed proximal or distal to the lesion, or both, is indicated for each injected axon. **I**: Distribution of the distances that giant RS axons regenerated beyond the center of the lesion scar (defined as 0 mm). Scale bar = 0.5 mm in B,C; 100 μm in D–G.

Alexa Fluor 488-phalloidin labeling and imaging of synapses

For labeling giant RS synapses within living control or transected lamprey spinal cords, giant RS axons were microinjected at positions proximal, within, and distal to the 5th gill/lesion scar with Alexa Fluor 488-conjugated phalloidin (Invitrogen) at a pipet concentration of 100 mM. Phalloidin strongly labels presynaptic sites at giant RS synapses by binding to a ring of filamentous actin (F-actin) that is associated with the synaptic vesicle clusters (Shupliakov et al., 2002; Morgan et al., 2004; Photowala et al., 2005; Bourne et al., 2006). As with HRP labeling, the phalloidin was delivered by small, repeated puffs of N_2 (10 ms; 0.3 Hz; 40 ppf). No additional TxRd was included in the pipet because Alexa Fluor 488-phalloidin itself is fluorescent and allows for visualization of the giant RS axon borders and their synapses.

For giant RS axons proximal to the lesion scar in transected spinal cords, the injections were performed at a distance of 1–2 mm above the center of the scar. According to previous studies, giant RS axons retract on average 1–2 mm after transection before they start to regenerate around 2–3 weeks post transection (Yin and Selzer, 1983; Zhang et al., 2005). Therefore, the presynaptic sites that were examined in the proximal axon segment at 10–12 weeks post transection were most likely a mixture of regenerated and remaining, original structures. In most cases, the proximal axons could be traced into or distal to the lesion scar by visually following the unbound Alexa Fluor 488-phalloidin. For axons distal to the lesion scar, the injections were typically performed 0.5–2 mm below the center of the scar. Then the identity of each axon as a regenerated giant RS axon was confirmed by tracing the unbound Alexa Fluor 488-phalloidin retrogradely through the lesion scar to a more proximal position. After presynaptic sites were labeled with Alexa Fluor 488-phalloidin, they were imaged by using a Zeiss LSM5 Pascal Exciter laser scanning confocal on an Axioskop 2FS upright microscope (Carl Zeiss Microimaging, Thornwood, NY). Specifically, images of phalloidin-labeled presynaptic structures were collected from small segments (75 μm in length) of giant RS axons within control and transected spinal cords at three locations: proximal, within, and distal to the 5th gill (i.e., the lesion site in transected spinal cords). To do so, serial confocal images were acquired through each axon segment using a 40×, 0.8 NA Zeiss Achroplan water-dipping objective. An additional 3× digital zoom was applied by using the Zeiss LSM v4.0 software. Next, the serial images were processed into a single 3-dimensional projection image, which was then used for quantitative analyses of the number, distribution, axonal density and complexity of presynaptic structures

within the giant RS axons. Only those presynaptic structures in which Alexa Fluor 488-phalloidin labeled a ring of F-actin with a visible center were counted in the analysis. Smaller, phalloidin-labeled puncta that did not fit this description were excluded because we could not be sure of their identity given our current knowledge.

Synapse density is defined as the number of phalloidin-labeled presynaptic structures within the 75-μm axon segment divided by the surface area of that same axon segment. Data were acquired from at least 10 axons proximal, within, and distal to the lesion scar at the level of the 5th gill in five to seven control or transected spinal cords. All analyses were performed by an experimenter who was not informed as to the experimental condition. Graphs were made and statistical analyses performed in Origin Pro 7.0 (OriginLab, Northampton, MA).

Immunofluorescence

For immunolabeling of giant RS synapses, spinal cords from control and transected lampreys were first fixed overnight in 4% PFA in 0.1 M PBS, pH 7.4. Then the spinal cords were cryoprotected by using serial sucrose infiltrations (12%, 15%, and 18% sucrose in 0.1 M PBS; >4 hours each at RT) and embedded horizontally in Tissue Freezing Medium (Electron Microscopy Sciences, Hatfield, PA). Longitudinal sections of frozen spinal cords were made at 20 μm (−22°C) by using a Microm HM 550 cryostat and mounted onto SuperFrost Plus slides (Fisher Scientific, Pittsburgh, PA). Immunofluorescence staining was performed as previously reported (Morgan et al., 2004). Spinal cord sections were incubated for 1 hour at RT in blocking buffer containing: 16% goat serum, 450 mM NaCl, 20 mM Na phosphate buffer (pH 7.4), and 0.3% Triton X-100. Sections were then incubated with primary antibodies against either synapsin (1:300) or synaptic vesicle glycoprotein 2 (SV2; 1:100) for 2 hours at RT.

The synapsin antibody, kindly provided by Drs. Ona Bloom and Paul Greengard, was a rabbit polyclonal generated by using a recombinant GST fusion of domain D of lamprey synapsin I (amino acids 470–635); it recognizes a doublet by Western blotting around 75 and 80 kDa, which are the predicted sizes for lamprey synapsin Ia and Ib (Pieribone et al., 1995; Kao et al., 1999; Bloom et al., 2003). This synapsin D domain antibody reliably immunolabels lamprey giant RS synapses (Morgan et al., 2004). The SV2 antibody was a mouse monoclonal, which was made by Dr. Kathleen Buckley and obtained from the Developmental Studies Hybridoma Bank (NICHD/University of Iowa, Iowa City, IA). This SV2 antibody was generated by using purified synaptic vesicles from the electric organ of the elasmobranch *Discopyge ommata* (Buckley and Kelly, 1985). It recognizes a major smeared band (due to glycosylation) around 90 kDa by Western blotting and reliably immunolabels synapses in all vertebrates tested, including lampreys (Bloom et al., 2003; Ono et al., 2004).

After primary antibody incubation, spinal cord sections were washed for 3 × 10 minutes in wash buffer (0.3% Triton X-100, 450 mM NaCl, 20 mM Na phosphate buffer, pH 7.4), followed by incubation in Alexa Fluor 488-conjugated goat anti-mouse or goat anti-rabbit IgG secondary antibodies (1:400; 60 minutes, RT; Invitrogen). Then spinal cord sections were washed for 3 × 10 minutes in wash buffer. Finally, sections were labeled with rhodamine phalloidin (Cytoskeleton, Denver, CO) at 1:300 for 45 minutes at RT, washed for 3 × 10 minutes in wash buffer, and coverslipped with Vectashield fluorescence mounting medium (Vector, Burlingame, CA). Images of presynaptic structures double-labeled with either synapsin or SV2 antibodies and with phalloidin were acquired by using a 40×, 1.3 NA EC Plan-Neofluar oil immersion objective and Zeiss LSM Pascal laser scanning confocal microscope.

Electron microscopy and ultrastructural analysis

Control or transected spinal cords were dissected and fixed overnight at RT in 3% glutaraldehyde, 2% paraformaldehyde diluted in 0.1 M sodium cacodylate buffer (pH. 7.4), as previously described (Morgan et al., 2004; Bourne et al., 2006). After fixation, spinal cords were washed in 0.1 M sodium cacodylate buffer (pH 7.4) for 3 × 10 minutes at RT and postfixed in 1% osmium tetroxide for 1 hour. Fixed spinal cords were then dehydrated via a graded ethanol series, infiltrated with 1:1 propylene oxide and Embed-812 resin overnight, and embedded in fresh resin for 48 hours at 60°C. All reagents were obtained from Electron Microscopy Sciences. Once embedded, thick (1-μm) sections, followed by a short series (5–10 sections) of ultrathin silver sections (70 nm), were obtained from control and transected spinal cords at 10–50-μm intervals. For transected spinal cords, sections were collected proximal, within, and distal to the 5th gill lesion scar. The thick sections were stained for 20–45 seconds with 1% toluidine blue in 1% sodium tetraborate, destained with distilled water, and coverslipped with Permount (Fisher Scientific) for imaging. This allowed us to select giant RS axons for tracing through the series and for examination of synapses. It also allowed us to identify the center of the lesion site with high precision (see Fig. 3E,F).

Ultrathin sections were placed on formvar-coated copper SynapTEK DOT slot grids (Ted Pella, Redding, CA), counterstained with 2% uranyl acetate and lead citrate, and imaged by using a Tecnai Spirit BioTwin T12 electron microscope (Tecnai, Hillsboro, OR) equipped with an Advanced Microscopy Techniques Advantage HS CCD camera (AMT, Danvers, MA). Within the preselected giant

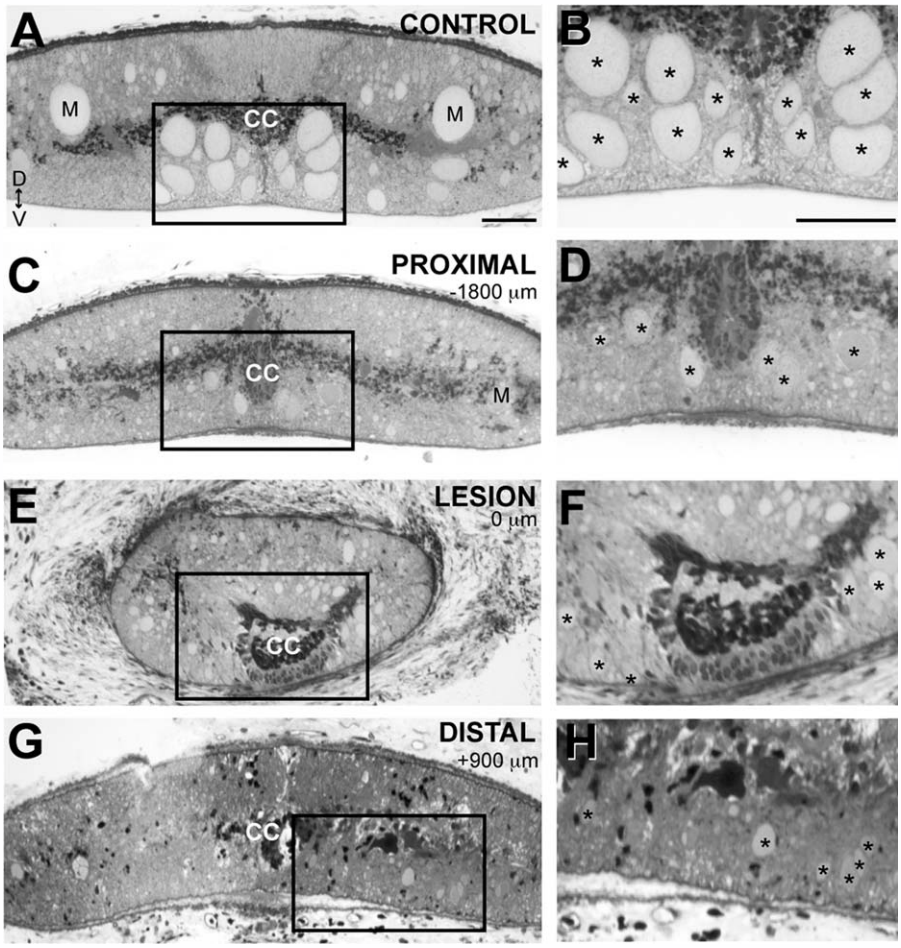

Figure 3. Sizes and locations of regenerated giant RS axons are altered. **A**: Brightfield image of a 1-μm cross section of a control spinal cord stained with toluidine blue. Most of the giant RS axons are located within the ventromedial region of the spinal cord (box), except for the Mauthner axons (M), which are located in the dorsolateral columns. Dorsal (D) and ventral (V) orientations are indicated. CC marks the central canal. **B**: Boxed region from A shown at higher magnification. Asterisks indicate the giant RS axons. **C–H**: Similar views of a lesioned spinal cord stained with toluidine blue at 12 weeks post-transection. Images were taken at locations proximal (C,D), in the center (E,F), and distal (G,H) to the lesion scar. Distances from the center of the scar are indicated. In the transected spinal cord, giant RS axons are smaller in diameter (asterisks), and many are absent from the ventromedial tract at all locations, due to prolonged axon retraction or regeneration into lateral areas. In E–H, the giant RS axons highlighted with asterisks were traced in serial sections from a position proximal to the lesion scar and are therefore regenerated giant RS axons. Scale bar = 50 μm in A (applies to A,C,E,G) and B (applies to B,D,F,H).

RS axons, each synaptic vesicle cluster was imaged at 26,500×. An experimenter, who was blinded to the experimental conditions, counted the number of vesicles and measured the active zone lengths from single ultrathin sections of synapses by using ImageJ software. Data were acquired from 18–35 synapses from at least 10 axons and 2 animals for each experimental condition. All graphs were made and statistical analyses performed in Origin Pro 7.0.

Photomicrograph production

All original micrographs were acquired as .tif or .jpg files. Within each experiment, the imaging conditions, including exposure, lighting, and gain, were kept constant. As a consequence, only slight modifications of contrast and brightness were needed, and these were performed in Adobe (San Jose, CA) Photoshop CS3. All figure layouts were generated by using Illustrator CS3. Final figures were exported from Illustrator as .tif files, which were subsequently cropped and sized in Photoshop according to journal standards.

RESULTS

Recovery of swimming in lampreys is robust after complete spinal cord transection

In order to place our measurements of synapse regeneration within a broader context of functional and structural recovery, we began by measuring the return of lampreys' swimming behaviors and the extent of axon

regeneration after SCI. It is well established that lampreys spontaneously recover nearly normal swimming behaviors within a few months after spinal transection (Fig. 1) (Rovainen, 1976; Cohen et al., 1986; Ayers, 1989; Davis et al., 1993). In our hands, the spinal-transected lampreys gradually regained undulatory swimming behaviors to a degree that was qualitatively difficult to distinguish from the behaviors of uninjured, control lampreys (Fig. 1A–D). Recovery of swimming movements across a population of spinal-transected lampreys was well described by an exponential process, reaching half maximum ($t_{1/2}$) at 3.2 ± 0.2 weeks post transection and nearing saturation at ~90% of normal levels by 10.5 weeks post transection and thereafter (Fig. 1E).

More detailed, quantitative measurements of the swimming kinematics measured from transected lampreys after 10 weeks of recovery revealed only mild differences in swim speed, tail beat frequency, and wavelength. Transected, recovered lampreys swam more slowly than uninjured, control lampreys (Fig. 1F,G; Control: 1.9 ± 0.1 L/s; Transected: 1.2 ± 0.1 L/s; Student's t-test; $P < 0.005$). Transected, recovered lampreys also used higher tail beat frequencies at a given swim speed (Fig. 1H), and their body wavelengths were shorter (Fig. 1I). Body wavelength (λ) is equal to twice the distance between successive peaks of curvature along the body (Fig. 1D). However, the changes in tail beat frequency and wavelength appeared to compensate for each other, because the body wave speed (approximately equal to the product of frequency and wavelength) was largely normal (Fig. 1J), if one accounts for the slower swim speed in transected animals. Wave speed is strongly related to both swimming speed and efficiency (Webb, 1975; Tytell and Lauder, 2004), and therefore is more functionally relevant than either frequency or wavelength alone. Thus, as previously reported, swimming was largely restored by 10–12 weeks post transection in lampreys.

Giant RS axons regenerate

After spinal transection, the proximal portions of giant RS axons retract for 1–2 weeks, and the distal portions degenerate; during the next few months, some of the axons regenerate across the lesion scar (Fig. 2A). Previous studies reported that 30–60% of the giant RS axons regenerate during this time frame (Rovainen, 1976; Wood and Cohen, 1981; Yin and Selzer, 1983; Davis and McClellan, 1993). Therefore, as a way to reveal the upper structural limits placed on synapse regeneration, we first determined the extent of giant RS axon regeneration in our experiments. To do so, giant RS axons from control spinal cords and transected spinal cords after 10–12 weeks of recovery were labeled by axonal microinjection of HRP, after which their morphologies were examined. As previously shown (Rovainen, 1967), control giant RS axons projected in fairly straight paths (Fig. 2B; n = 41 axons, 9 spinal cords) and were located predominantly within the ventromedial spinal cord (Fig. 3A,B). In contrast, giant RS axons within transected spinal cords were smaller and projected within both medial and lateral tracts (Figs. 2C, 3C–H). At 10–12 weeks after transection, giant RS axons also exhibited a variety of atypical structures, including early termination, branching, rostral turning, and midline crossing, which occurred both proximal and distal to the lesion scar (Fig. 2D–H; n = 51 axons, 17 spinal cords). Out of 51 HRP-labeled giant RS axons within transected spinal cords, 22 (or 43%) regenerated distal to the center of the scar. The average distance of axon regeneration was 2.0 ± 0.4 mm with a maximal distance of 5.4 mm (Fig. 2I). These data are in excellent agreement with those of previous studies, and they provided a broader structural context in which to place our subsequent evaluation of synapse regeneration.

Regenerated giant RS axons produce very few presynaptic structures

We next moved to the main goal of determining the extent of synapse regeneration within regenerated giant RS axons. To this end, we began by imaging presynaptic structures within living giant RS axons of control spinal cords and transected spinal cords after 10–12 weeks of recovery. Giant RS axons normally produce large en passant synapses that are located around the circumference of the axolemma (Fig. 4A, left inset). Presynaptic sites within control giant RS axons can be labeled reliably by axonal microinjection of Alexa Fluor 488-conjugated phalloidin, which binds to a ring of filamentous actin (F-actin) associated with synaptic vesicle clusters (Fig. 4A, middle and right insets) (Shupliakov et al., 2002; Morgan et al., 2004; Bourne et al., 2006). To quantify and compare presynaptic sites within control and regenerated giant RS axons, we therefore microinjected Alexa Fluor 488-phalloidin at locations proximal, within, or distal to the 5th gill (or lesion scar; see Fig. 2B,C for locations). We note that presynaptic sites within axons proximal to the lesion scar in transected spinal cords are likely a mixture of regenerated and original structures, whereas those within and distal to the lesion scar are all regenerated. A more detailed explanation is provided in Materials and Methods.

In control giant RS axons, phalloidin-labeled presynaptic sites appeared to be equally abundant at all locations (Fig. 4B–D). Similarly, in transected spinal cords, presynaptic sites were abundant within the giant RS axon proximal to the lesion (Fig. 4E). In stark contrast, presynaptic

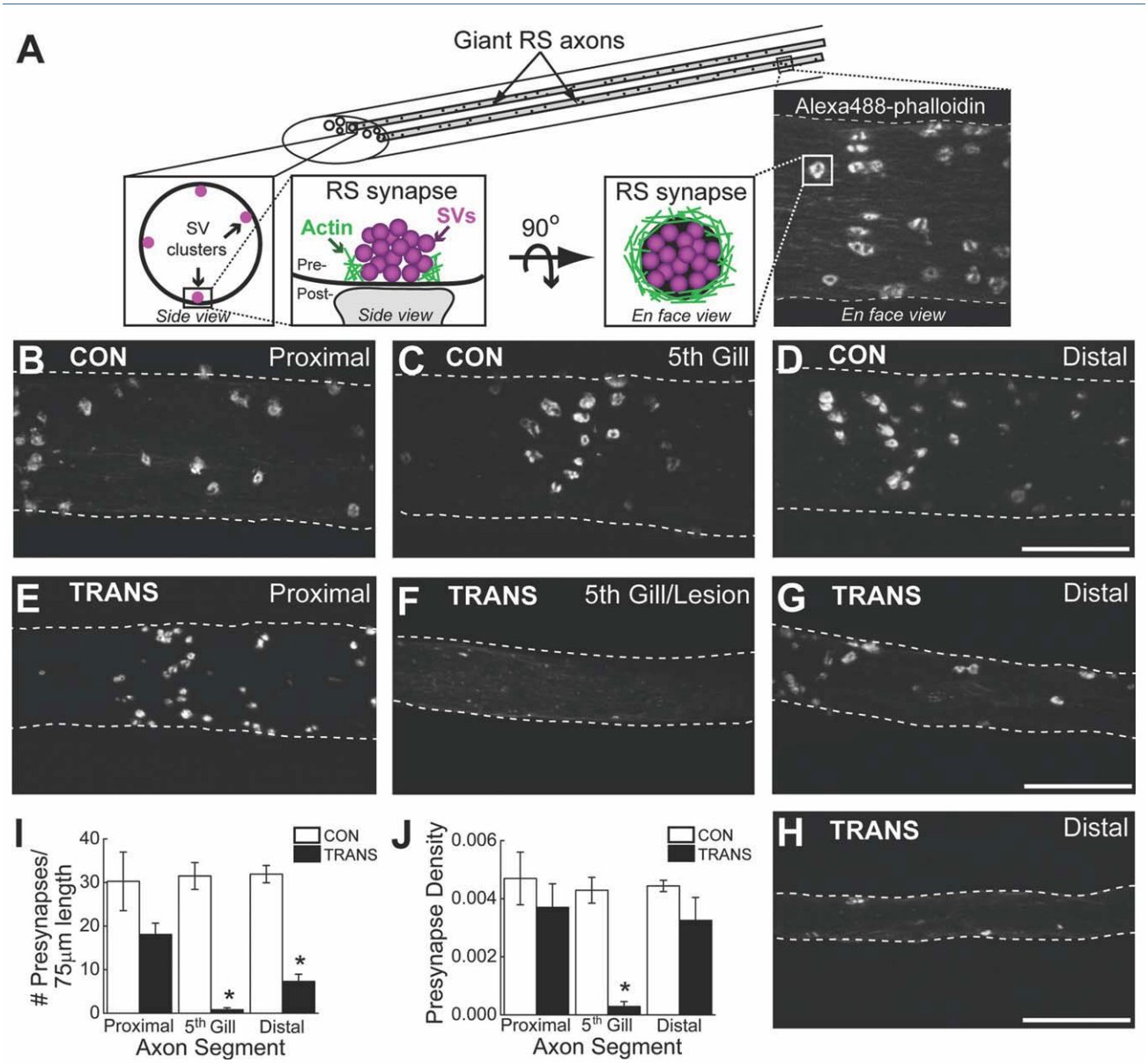

Figure 4. Very few presynaptic sites are found in regenerated giant RS axons. **A**: Diagram showing the organization of presynaptic sites within control giant RS axons. Synaptic vesicle (SV) clusters are located around the circumference of giant axons (left inset). Each presynaptic site consists of a large SV cluster associated with a dense ring of F-actin (middle insets), which can be labeled by axonal microinjection of Alexa Fluor 488-phalloidin (right inset). **B–H**: Confocal projection images of Alexa Fluor 488-phalloidin-labeled presynaptic sites within live giant RS axons of control (CON) (B–D) and transected (TRANS) (E–H) spinal cords after 10–12 weeks of recovery. Images were taken at positions proximal, within, and distal to the 5th gill/lesion scar. White rings demark the fluorescently labeled presynaptic sites. There was no obvious difference in the number of presynaptic sites throughout all regions of control RS axons and proximal regions of transected axons. In contrast, regenerated giant RS axons within and distal to the lesion scar produced fewer presynapses. Hatched lines indicate axon borders. **I,J**: Quantification of the imaging data revealed a significant reduction in the number of presynaptic sites within regenerated giant RS axons (I). However, the density of presynaptic sites along the distal regenerated axons was partially restored (J). Presynapse density is measured as the number (of presynapses) per μm^2 of axonal surface area. Bars indicate the mean ± SEM. Asterisks indicate statistical significance. Scale bar = 20 μm in D (applies to B–D), G (applies to e–G), and H.

sites were nearly absent within the 5th gill/lesion segments of regenerated giant RS axons (Fig. 4F), and only a few were observed within distal regenerated axons (Fig. 4G,H). Quantification of these data revealed that the number of presynaptic sites was uniform throughout the control giant RS axons but significantly reduced in giant RS axons of transected spinal cords (Fig. 4I; $P < 0.001$; ANOVA). Specifically, RS axons proximal to the lesion in transected spinal cords contained 60% of the typical number of presynaptic sites seen in the same location in

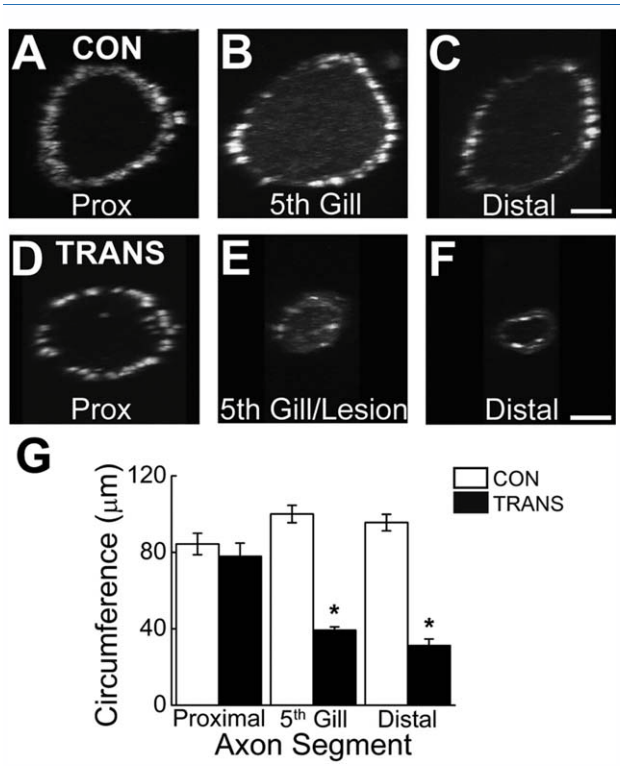

Figure 5. Regenerated giant RS axons have smaller circumferences. **A–F**: Confocal projection images of living giant RS axons within control (A–C) and transected (D–F) spinal cords, which were injected with Alexa Fluor 488-phalloidin as in Figure 4 and rotated 90° around the vertical axis. **G**: The rotation images were used for measurements of axon circumference. Note the small size of regenerated giant RS axons (5th gill, distal) in transected spinal cords. Circumference measurements were then used to calculate axonal surface area, which was necessary for determining presynapse density in Figure 4J. Bars indicate the mean ± SEM. Asterisks indicate statistical significance. Scale bar = 10 μm in C (applies to A–C) and F (applies to D–F).

control axons, but this decrease was not statistically significant ($Control_{(PROXIMAL)}$ 30.3 ± 6.8, n = 11 axons; $Transected_{(PROXIMAL)}$: 18.1 ± 2.6; n = 13 axons; $P > 0.05$; Tukey's). However, regenerated RS axons traversing the 5th gill/lesion scar of transected spinal cords contained only 3% of the normal number of presynaptic sites ($Control_{(5th\ GILL)}$: 31.5 ± 3.1; n = 18 axons; $Transected_{(5th\ GILL)}$: 0.8 ± 0.5; n = 10 axons; $P < 0.05$; Tukey's). Although presynaptic sites were visible in distal regenerated RS axons, the number was significantly reduced to only 23% of control values ($Control_{(DISTAL)}$: 31.9 ± 2.0; n = 13 axons; $Transected_{(DISTAL)}$: 7.3 ± 1.7; n = 10 axons; $P < 0.05$; Tukey's). Thus, regenerated giant RS axons produced very few presynapses, compared with the normal number typically observed within these axons, especially within and beyond the lesion scar.

The axonal density of presynaptic sites is nearly restored in distal regenerated giant RS axons

Not only the absolute number, but also the density, of presynaptic contacts onto their targets strongly influences the postsynaptic responses (Magee, 2000; Spruston, 2008). Therefore, we examined the density of presynaptic sites within giant RS axons of transected spinal cords after 10–12 weeks of recovery and compared it with the presynaptic density in control giant RS axons. Here, presynapse density is defined as the number of presynaptic sites in a short (75-μm) giant RS axon segment divided by the surface area of that same axon segment. Practically, this was determined by dividing the number of presynaptic sites in each axon segment shown in Figure 4B–H by the estimated surface area (SA) of that same axon segment, where SA = axon circumference × axon length (75 μm). Axon circumference was easily obtained by rotating the projection images by 90° (Fig. 5A–F). Notably, the average circumference of regenerated giant RS axons was significantly lower than that of control axons or axons proximal to the lesion site (Fig. 5G; $P < 0.0005$; ANOVA).

Overall, presynaptic density was significantly different in giant RS axons of control and transected spinal cords (Fig. 4J; $P < 0.0005$; ANOVA). However, synapse density was not significantly different in axons proximal to the lesion of transected spinal cords, where the density of presynaptic sites reached 79% of control values ($Control_{(PROXIMAL)}$: 0.0047 ± 0.0009 synapses/μm^2, n = 11 axons; $Transected_{(PROXIMAL)}$: 0.0037 ± 0.0008 synapses/μm^2; n = 13 axons; $P > 0.05$; Tukey's). As expected, because there were virtually no synapses in this location, the presynapse density was significantly reduced to only 7% of control values in 5th gill/lesion segments of regenerated RS axons ($Control_{(5th\ GILL)}$: 0.0043 ± 0.0008 synapses/μm^2, n = 18 axons; $Transected_{(5th\ GILL)}$: 0.0003 ± 0.0002 synapses/μm^2, n = 10 axons; $P < 0.05$ Tukey's). Interestingly, once regenerated giant RS axons grew distal to the lesion site, presynapse density returned to 75% of control levels, a difference that was not statistically significant ($Control_{(DISTAL)}$: 0.0044 ± 0.0002 synapses/μm^2, n = 13 axons; $Transected_{(DISTAL)}$: 0.0033 ± 0.0008 synapses/μm^2, n = 10 axons; $P > 0.05$; Tukey's). Thus, despite a large reduction in the total number of presynaptic sites within regenerated giant RS axons, the presynapse density was partially restored as a result of changes in axon circumference.

Presynaptic sites within regenerated giant RS axons are simpler than normal

We next evaluated the higher order structures of the presynaptic sites within giant RS axons of control and

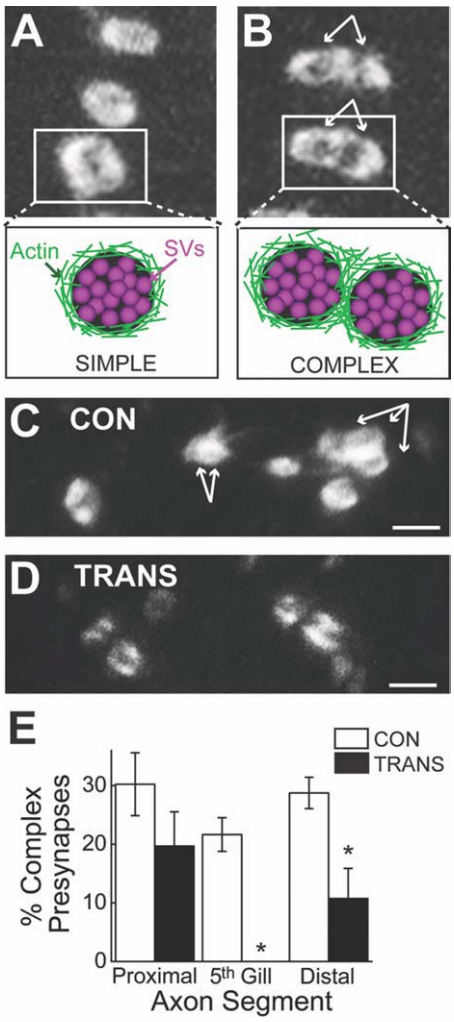

Figure 6. Regenerated RS synapses have simpler structures. **A,B**: High-magnification confocal images showing examples of simple (A) and complex (B) presynaptic sites within living giant RS axons labeled with Alexa Fluor 488-phalloidin. The bundled white arrows indicate the number and positions of multiple F-actin rings comprising each complex presynaptic site. **C,D**: Confocal images showing a small population of presynaptic sites within a giant RS axon of a control (CON; C) or a transected (TRANS; D) spinal cord. Whereas giant RS axons of control spinal cords typically contained several complex presynaptic sites, complex presynapses were rarely observed in giant RS axons of transected spinal cords. **E**: Regenerated giant RS axons produced proportionally fewer complex presynaptic sites than the typical number. Bars indicate the mean ± SEM. Asterisks indicate statistical significance. Scale bar = 2 μm in C,D.

transected spinal cords. To do so, we measured the proportion of simple presynaptic sites, which we defined as single Alexa Fluor 488-labeled F-actin rings (Fig. 6A), versus complex presynaptic sites, which we defined as groups of F-actin rings sharing part of their borders in common (Fig. 6B). Within control giant RS axons, complex presynaptic sites appeared frequently (Fig. 6C). Within giant RS axons of transected spinal cords, however, complex presynaptic sites were rarely observed (Fig. 6D). A quantitative comparison revealed that regenerated giant RS axons produced proportionally fewer complex presynaptic sites in comparison with those in control giant RS axons (Fig. 6E; $P < 0.00005$; ANOVA). Although the percentage of complex presynaptic sites was reduced to 65% of control values within axons proximal to the lesion site, this difference was not statistically significant ($Control_{(PROXIMAL)}$: 30.2 ± 5.3%; n = 11 axons; $Transected_{(PROXIMAL)}$: 19.7 ± 5.8%; n = 13 axons; $P > 0.05$; Tukey's).

In contrast, there was a complete loss of complex presynaptic sites within the regenerated giant RS axons traversing the 5th gill/lesion scar of transected spinal cords ($Control_{(5th\ GILL)}$: 21.6 ± 2.9%; n = 18 axons; $Transected_{(5th\ GILL)}$: 0 ± 0%; n = 10 axons; $P < 0.05$; Tukey's). Within distal regenerated giant RS axons the proportion of complex presynaptic sites was significantly reduced to only 37% of control values ($Control_{(DISTAL)}$: 28.7 ± 2.7%; n = 13 axons; $Transected_{(DISTAL)}$: 10.7 ± 5.1%; n = 10 axons; $P < 0.05$; Tukey's). Thus, regenerated giant RS axons produced presynaptic sites with simpler structures than those typically observed in control giant RS axons.

A typical presynaptic organization is restored at regenerated giant RS synapses

Next, we examined whether Alexa Fluor 488-labeled presynaptic sites reliably reported the locations of synaptic vesicle clusters within regenerated giant axons, as is the case in control axons (Fig. 4A). Using immunofluorescence on frozen spinal cord sections, presynaptic sites were double-labeled with fluorescent phalloidin and antibodies against either synapsin or SV2, two abundant synaptic vesicle proteins (Bloom et al., 2003; Morgan et al., 2004). As previously reported (Shupliakov et al., 2002; Evergren et al., 2007), each F-actin ring in control RS axons was associated with a synaptic vesicle cluster, as shown by co-localization with either synapsin (Fig. 7A–C) or SV2 (Fig. 7D–F). Similarly, in distal regenerated giant RS axons, the F-actin rings were closely associated with synapsin (Fig. 7G–I) and SV2 (Fig. 7J–L), indicating that phalloidin is indeed a reliable marker of vesicle clusters at regenerated synapses. Thus, most presynaptic sites within regenerated giant RS synapses regained a typical organization and contained several of the major molecular components: actin, synapsin, and SV2. However, in regenerated giant RS axons, the synaptic vesicle clusters often appeared smaller and more variable in size (Fig. 7H,K). Furthermore, an occasional synapsin-positive punctum that was not associated with F-actin was also observed (Fig. 7H,I, arrow), introducing the possibility

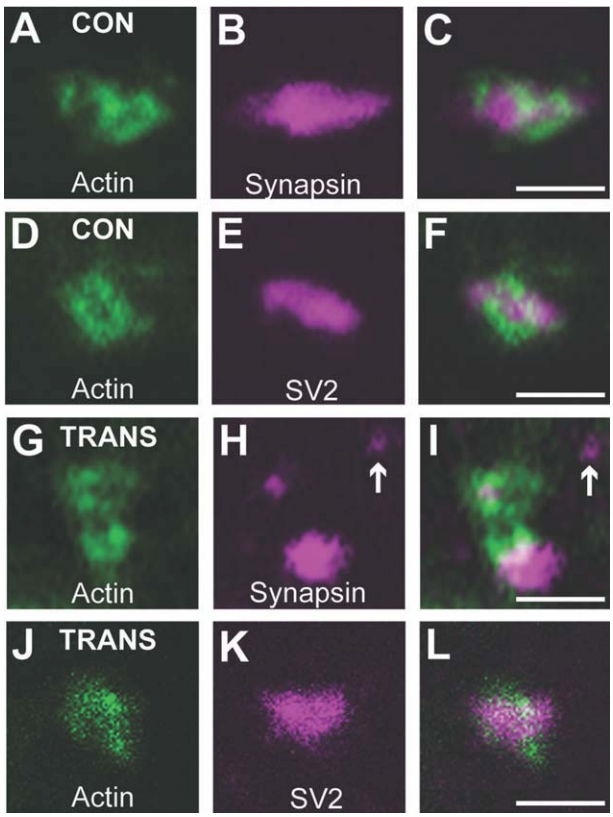

Figure 7. Regenerated synapses regain a typical presynaptic organization. **A–C**: Confocal image of a complex presynaptic site within a control giant RS axon, which was double-labeled with phalloidin (A) to mark the F-actin ring and a synapsin antibody (B) to mark the synaptic vesicle clusters. **D–F**: A simple presynaptic site within a control giant RS axon, which was double-labeled with phalloidin (D) and an antibody against SV2 (E), another vesicle marker. Note that the phalloidin rings always corresponded to the location of a synaptic vesicle cluster. **G–L**: Presynaptic sites within distal regenerated giant RS axons, which were double-labeled with phalloidin and either the synapsin antibody (G–I) or the SV2 antibody (J–L). As in control giant RS synapses, the actin ring at regenerated presynapses corresponded to the location of a synapsin- or SV2-positive synaptic vesicle cluster. However, the vesicle clusters appeared more variable in size, and additional synapsin-positive puncta were occasionally observed (arrow). Scale bar = 2 μm in C (applies to A–C), F (applies to D–F), I (applies to G–I), and L (applies to J–L).

that regenerated RS axons may contain additional presynaptic sites that could not be resolved properly using light microscopy. Therefore, we turned to electron microscopy for a more detailed examination of regenerated giant RS synapses.

Regenerated RS synapses lack gap junctions and have simpler structures

Most control giant RS synapses have simple presynaptic structures, consisting of a single, large vesicle cluster roughly centered around an electron-dense active zone and apposing a single postsynaptic element (Fig. 8A) (Wickelgren et al., 1985; Gustafsson et al., 2002). Also observed in control giant RS axons are complex presynaptic structures, comprising either multiple vesicle clusters and active zones apposed to one or more postsynaptic dendrites (Fig. 8B), or a single, fused vesicle cluster with multiple active zones and postsynaptic dendrites (not shown; see Gustafsson et al., 2002). Similar to what was previously reported for distal regenerated axons (Wood and Cohen, 1979, 1981; Lurie et al., 1994), we found that all giant RS synapses within axons proximal and distal to the lesion contained an identifiable SV cluster, active zone, and postsynaptic dendrite, indicating that the basic structural components of the chemical synapse were restored (Fig. 8C,D). In addition, synapses within small sprouts protruding from the surface of the axolemma were observed (not shown; 3 of 19 proximal; 3 of 18 distal) (Wood and Cohen, 1981; Lurie et al., 1994), but these were uncommon. Presynaptic specializations (i.e., vesicle clusters and active zones) without postsynaptic dendrites were never observed. In general, synaptic vesicle clusters and active zones of regenerated RS synapses appeared smaller than normal.

Of all the giant RS synapses imaged in control axons, 31% (12 of 39) had complex presynaptic structures. Only 11% (2 of 19) and 22% (4 of 18) of synapses within axons proximal and distal to the lesion, respectively, had complex presynaptic structures. Thus, at the ultrastructural level, regenerated giant RS synapses had simpler presynaptic structures, a finding that is consistent with our light microscopic analysis (Fig. 6D,E). By our sampling method, only 5% (1 of 19) of synapses within proximal axons contained a gap junction adjacent to the SV cluster, whereas 18% (7 of 39) of control synapses had them (Fig. 8E,F). No gap junctions were observed at distal regenerated synapses (0 of 18), as previously reported (Wood and Cohen, 1981; Mackler and Selzer, 1987). Taken together, although regenerated giant RS synapses regained all the basic structural features of chemical synapses, they had less complex structures and largely lacked gap junctions.

Synapses within giant RS axons proximal and distal to the lesion are smaller but have normal densities of docked SVs

To quantify any differences in the ultrastructural features of giant RS synapses within control and transected spinal cords, we measured the total number of synaptic vesicles, the number of docked synaptic vesicles, and the active zone lengths from individual sections. Whereas docked vesicles are those that are in direct contact with the presynaptic plasma membrane and that functionally correspond to the readily releasable pool, the remaining

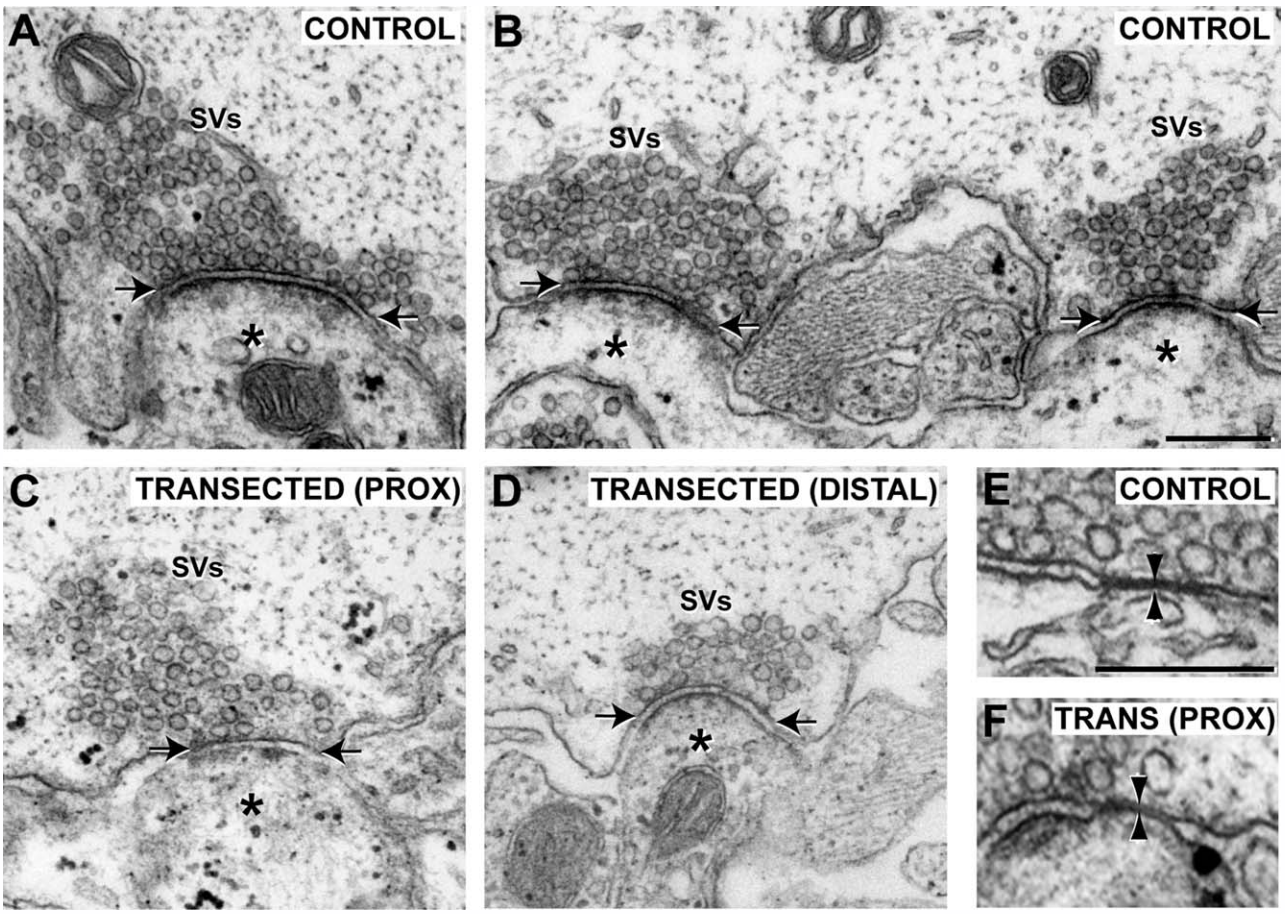

Figure 8. Giant RS synapses within proximal and distal axons regain the basic features of chemical synapses. **A,B**: Electron micrographs of control giant RS synapses with simple (A) or complex (B) presynaptic structures. In all cases, synapses contain a large cluster of synaptic vesicles (SVs) and an electron-dense active zone (between arrows), and they are directly apposed to a postsynaptic dendrite (asterisk). **C,D**: Giant RS synapses within axons proximal (C) and distal (D) to the lesion scar after 12 weeks of recovery also exhibited typical features of chemical synapses. However, SV clusters and active zones often appeared smaller, and complex presynaptic structures were rarely observed. **E,F**: At control synapses, gap junctions (between arrowheads) were often seen adjacent to the chemical synapses (E). Shown here is the only gap junction observed at a giant RS synapse within an axon proximal to the lesion (F). Scale bar = 250 nm in B (applies to A–D) and E (applies to E,F).

majority of vesicles comprise the reserve pool that is drawn upon during high levels of activity (Pieribone et al., 1995; Murthy et al., 2001; Rizzoli and Betz, 2005). On average, synapses within giant RS axons of transected spinal cords (10 weeks post transection) had fewer total synaptic vesicles than is observed at control synapses (Fig. 9A; $P < 0.0005$; ANOVA). Within axons proximal and distal to the lesion in transected spinal cords, the average number of vesicles per section was significantly reduced to 56% and 47% of control values, respectively (Fig. 9A; Control: 110 ± 48 SVs, n = 35; $\text{Transected}_{(\text{PROXIMAL})}$: 62 ± 43 SVs, n = 19; $\text{Transected}_{(\text{DISTAL})}$: 52 ± 23 SVs, n = 18; $P < 0.05$; Tukey's).

Similarly, the number of docked vesicles was reduced to 56% and 67% of control values at synapses proximal and distal to the lesion scar (Fig. 9B; $P < 0.005$; ANOVA; Control: 8.8 ± 0.9 docked SVs; $\text{Transected}_{(\text{PROXIMAL})}$: 4.9 ± 0.6 docked SVs; $\text{Transected}_{(\text{DISTAL})}$: 5.9 ± 0.5 docked SVs; $P < 0.05$ Tukey's). In addition, the average active zone (AZ) length only reached 66% and 72% of control values, respectively, at synapses proximal and distal to the lesion (Fig. 9C; $P < 0.005$; ANOVA; Control: 0.53 ± 0.04 μm; $\text{Transected}_{(\text{PROXIMAL})}$: 0.35 ± 0.04 μm; $\text{Transected}_{(\text{DISTAL})}$: 0.38 ± 0.04 μm; $P < 0.05$ Tukey's).

At control giant RS synapses of adult lampreys (*Lampetra fluviatilis*), there is a strong positive correlation between the size of the synaptic vesicle cluster and the active zone length (Gustafsson et al., 2002). Therefore, we wanted to determine whether this relationship exists at control giant RS synapses of larval lampreys of the species used in this study (*Petromyzon marinus*) and, if so, whether it persists at regenerated synapses. At control synapses, there was a weak positive correlation between the total number of synaptic vesicles and the size of the active zone (Fig. 9D; Control: r = 0.19). Synapses both proximal and distal to the lesion exhibited a similar weak,

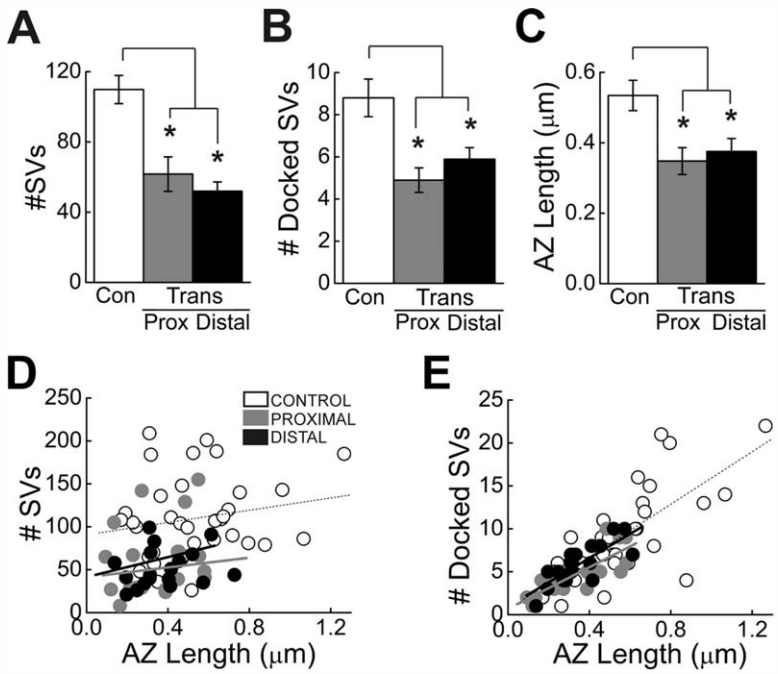

Figure 9. Regenerated giant RS synapses are smaller than normal. A–C: Giant RS synapses within proximal and distal axons have fewer total SVs (A), fewer docked SVs (B), and shorter active zones (C) than control synapses, as measured from individual thin sections. Bars indicate mean ± SEM. Asterisks indicate statistical significance. D,E: Scatter plots showing the relationship between the total number of SVs (D) or docked SVs (E) and the AZ length at giant RS synapses of control, proximal, and distal axons. Data points indicate measurements from individual synapses, and lines represent best fits. For any given AZ length, the synapses in regenerated axons typically had fewer total SVs than control synapses (D). However, the density of docked SVs was normal (E).

positive correlation (Fig. 9D; Proximal: r = 0.23; Distal: r = 0.19). At 10–12 weeks of recovery, giant RS synapses within proximal or distal axons did not contain more than 155 synaptic vesicles or active zones longer than 0.73 μm. Furthermore, for any given active zone length, the total number of synaptic vesicles at proximal and distal giant RS synapses was usually smaller.

In contrast, there was a strong positive correlation between the number of docked synaptic vesicles and active zone length at giant RS synapses of control and transected axons (Fig. 9E, Control: r = 0.74; Proximal: r = 0.79; Distal: r = 0.79). Notably, although synapses within proximal and distal axons had smaller active zones, the density of docked synaptic vesicles (number of SVs per micrometer of AZ length) was normal for their small size (Fig. 9E). Thus, by several measurements, regenerated giant RS synapses were smaller than control giant RS synapses but had a normal density of docked SVs.

Ultrastructural analysis confirmed the paucity of regenerated giant RS synapses

In order to quantify the number of regenerated giant RS synapses by a second independent method, we used a semiserial sampling method combined with EM. We first generated five sets of sections from control (n = 2) and transected spinal cords at 12 weeks post transection (n = 2), which were spaced at 50-μm intervals (Fig. 10A). Each set contained a 1-μm-thick section followed by several

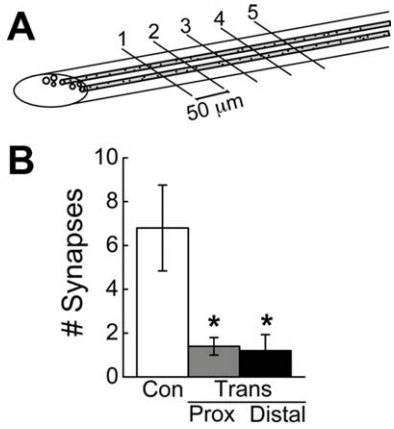

Figure 10. EM analysis confirms the small number of regenerated RS synapses. A: Diagram showing the semi-serial sectioning approach used to determine the relative number of synapses in giant RS axons of control and transected spinal cords. B: Compared with control giant RS axons, there are significantly fewer synapses in axons located proximal and distal to the lesion. No synapses were observed within the lesion scar. Bars indicate mean ± SEM. Asterisks indicate statistical significance.

ultrathin sections. The thick sections were stained with toluidine blue and used for selection of five giant RS axons that could be traced reliably through the entire series. Then the number of giant RS synapses within each preselected axon was determined by imaging the ultrathin sections with EM. On average, giant RS axons proximal and distal to the lesion had dramatically fewer synapses compared with axons in control spinal cords (Fig. 10B; $P < 0.05$; ANOVA). Proximal and distal RS axons within transected spinal cords produced only 21% and 18% of the number of synapses, respectively compared with control axons (Control: 6.8 $\pm$ 2.0 synapses; $\text{Transected}_{(\text{PROXIMAL})}$: 1.4 $\pm$ 0.4 synapses; $\text{Transected}_{(\text{DISTAL})}$: 1.2 $\pm$ 0.7 synapses; $P < 0.05$; Tukey's). Synapses were never observed within the lesion site. Taken together, these data corroborate a primary observation of this study, which is that regenerated giant RS axons produce only a small number of synapses despite the high degree of functional recovery.

DISCUSSION

Although regenerated giant RS synapses regain many typical features of chemical synapses, some differences remain

Previous studies first demonstrated that several months after spinal cord transection giant RS axons proximal and distal to the lesion contained chemical synapses with typical features, such as a vesicle cluster, an active zone, and a postsynaptic dendrite (Wood and Cohen, 1979, 1981; Lurie et al., 1994). However, the gap junctions, or electrotonic potentials, that normally exist at these mixed giant RS synapses were not observed in regenerated axons (Wood and Cohen, 1981; Mackler and Selzer, 1987). Data presented here confirm the previous findings. That is, we also observed that the large vesicle clusters within proximal and distal axons were always associated with proper chemical synapses (Fig. 8). We did detect a single gap junction within a giant RS axon proximal to the lesion in a transected spinal cord (Fig. 8F). However, because we do not know how far the giant RS axon degenerated in the first few weeks after transection, it is not possible to determine whether this gap junction was at an original synapse or a newly regenerated one. We observed gap junctions at only 18% of control giant RS synapses, whereas previous studies reported gap junctions or electrotonic potentials at virtually all of them (Brodin et al., 1994; Gustafsson et al., 2002). A likely explanation for this discrepancy is the difference in sampling methods. In the previous EM study, serial sections were acquired through entire synapses (Gustafsson et al., 2002), whereas we used shorter series of 5–10 sections, making it likely that the gap junctions were simply out of the sectioning plane. However, by our sampling method, we still detected very few gap junctions in axons proximal and distal to the lesion, confirming previous reports (Wood and Cohen, 1981; Mackler and Selzer, 1987) that the electrical component of giant RS synapses does not regenerate normally by 10–12 weeks post-transection.

The findings presented here also extend our knowledge of the basic characteristics of regenerated giant RS synapses and reveal several key similarities between them and control synapses. First, presynaptic sites within distal regenerated giant RS axons regained several key molecular players that are found at all vertebrate synapses: actin, synapsin, and SV2 (Fig. 7). Actin is tightly associated with the vesicle cluster, typically at the periactive zone, and it is important for vesicle recycling and molecular scaffolding (Shupliakov et al., 2002; Sankaranarayanan et al., 2003; Richards et al., 2004; Bourne et al., 2006). Synapsin and SV2 are two of the most abundant proteins on synaptic vesicles, and both are required for proper transmitter release (Pieribone et al., 1995; Janz et al., 1999; Takamori et al., 2006). Second, the presence of actin rings that surround synapsin- and SV2-containing vesicle clusters at regenerated synapses indicates that the basic presynaptic organization is restored (Fig. 7), a finding that is corroborated by the ultrastructural analyses (Figs. 8, 9). Third, the regenerated synapses contained the normal density of docked vesicles (Fig. 9E), which correlate functionally to the readily releasable pool (Murthy et al., 2001; Rizzoli and Betz, 2005). Taken together, these data are suggestive that the regenerated synapses are functional, but demonstrating this conclusively will require further experiments.

Despite the similarities between giant RS synapses within control and transected spinal cords, some measurable differences remain. Synapses within giant RS axons proximal and distal to the lesion had significantly smaller vesicle clusters and active zones than control giant RS synapses (Figs. 8, 9). The majority of this loss is from the reserve pool, which is typically employed at high levels of activity (Pieribone et al., 1995; Hilfiker et al., 1999; Rizzoli and Betz, 2005). In addition, proximal and distal axons produced synapses with proportionally fewer complex presynaptic structures, based on the distribution of F-actin rings and synaptic vesicles (Figs. 6, 8). Taken together, it is possible that newly regenerated giant RS synapses may initially form as small, simple synapses with an appropriate density of docked vesicles and that the size of the reserve pool and the complexity of these synapses increase over time, as occurs during developmental synaptogenesis (Ahmari et al., 2000; Ziv and Garner, 2004; Nagerl et al., 2007). However, an analysis of synapse formation at shorter and longer axon regeneration times, including a careful examination of postsynaptic

targets, will be required to elucidate the cellular mechanisms by which regenerated synapses form and mature.

The population of regenerated giant RS synapses is vanishingly small after recovery from SCI

One model for restoring synapse function would be for the regenerating axon to recapitulate the same number and organization of synapses as in the original axon. This seems to occur after crush injury in the peripheral nervous system, where regenerating motor axons precisely reinnervate their original muscle fiber targets (Son and Thompson, 1995; Nguyen et al., 2002; Lichtman and Sanes, 2003). However, our data do not support this model as a mechanism for regenerating giant RS synapses. Instead, distal regenerated giant RS axons grew in unusual locations (Figs. 2, 3) and produced fewer synapses (Figs. 4, 10) in comparison with control axons. An alternative model for restoring synaptic function would be via a homeostatic compensation of both synaptic structures and strength. For example, regenerating giant RS axons could produce a smaller number of synapses than normal, each with enhanced synaptic strength (Rich and Wenner, 2007). There is some growing support for this idea, as discussed below.

The total number of synapses produced by a population of neurons is a basic indicator of the potential that the neurons have for providing input to downstream targets. Therefore, to gain a better understanding of the potential that the regenerated giant RS axons have for transmitting synaptic input to the downstream locomotor network, we have extrapolated our findings on synapse numbers to include the entire population of regenerated giant RS axons. Indeed, the result is quite surprising. Within each distal regenerated giant RS axon, the average number of synapses was only 18% (Fig. 10B; EM analysis) or 23% (Fig. 4E–H; phalloidin staining) of control values. However, only about half of the giant RS axons regenerate to positions distal to the lesion site at 10–12 weeks post-transection (Rovainen, 1976; Yin and Selzer, 1983; Davis and McClellan, 1993). The other giant RS neurons do not regenerate because they undergo a delayed death (Shifman et al., 2008). Thus, the number of regenerated synapses immediately distal to the lesion is reduced to roughly between 9% (half of 18%) and 11.5% (half of 23%) of control values. In addition, whereas control giant RS axons extend along the entire length of the lamprey, regenerated axons terminate within several millimeters distal to the lesion scar, further reducing the population of regenerated giant RS synapses. In this study, the longest distance of giant RS axon regeneration was 5.4 mm (Fig. 2I), a value that corresponds well with previous measurements (Rovainen, 1976; Yin and Selzer, 1983; Davis and McClellan, 1994). Therefore, by ~5–6 mm distal to the lesion scar, the total population of regenerated giant RS synapses was nearly or completely absent. Given that the giant RS axons would ordinarily extend for another 5–10 cm in these late larval stage lampreys, our best estimate is that the spinal cord regenerates only 1–2% of the giant RS synapses by 10–12 weeks post transection.

Injury-induced plasticity in the lamprey spinal cord is diverse and complex

Despite the paucity and small size of regenerated giant RS synapses (Figs. 4, 8–10), functional recovery of swimming is robust and nearly complete (Fig. 1). What are some possible explanations for this finding? Under normal conditions, giant RS neurons belong to a larger population of ~1,200 descending command neurons that together initiate and modulate a variety of locomotor behaviors, including swimming, turning, crawling, and postural control (Orlovsky et al., 1992; Deliagina et al., 2000; Buchanan, 2001; Zelenin, 2005; Dubuc et al., 2008). After spinal cord transection, blocking axon regeneration by removing several millimeters of the spinal cord prevents recovery of swimming (Jacobs et al., 1997). However, this manipulation would also block the growth of other types of axons that regenerate across the lesion scar and that might contribute to functional recovery, including both smaller and giant RS axons, sensory neurons, and interneurons (Yin and Selzer, 1983; McClellan, 1994; Buchanan, 2001). Therefore, to properly understand the contribution that regenerated giant RS synapses play during functional recovery would require a selective perturbation of giant RS axon regeneration, followed by re-evaluation of the swimming kinematics. Although the precise role for regenerated giant RS synapses remains unclear, the data presented here suggest that only a small number are needed.

Other compensatory changes within the lesioned spinal cord have been identified that could facilitate the recovery of swimming, despite the low number of regenerated RS synapses. First, transection induces a great deal of plasticity throughout the spinal cord and brain. For example, spinal transection changes levels and distribution of neuromodulators and alters intrinsic properties of both descending and spinal neurons (Cohen et al., 2005; McClellan et al., 2008; Cooke and Parker, 2009). Furthermore, injury induces compensatory changes in the synaptic properties of excitatory interneurons below the lesion, such that both the amplitudes and frequencies of miniature excitatory postsynaptic potentials (EPSPs) increase (Cooke and Parker, 2009). Other sources of plasticity

likely exist that have yet to be identified. Second, the small number of regenerated synapses may be compensated for by increasing their synaptic strength (Rich and Wenner, 2007). Indeed, unusually large EPSPs have been observed at a subset of regenerated giant RS synapses after recovery from spinal cord injury (Mackler and Selzer, 1987; Cooke and Parker, 2009). At first, this may seem at odds with the morphological characteristics of the small, sparsely regenerated giant RS synapses that we observed. However, one plausible explanation is that the synaptic release probability is increased in regenerated giant RS axons, such that a greater proportion of the viable synapses releases transmitter with each action potential. Alternatively, giant EPSPs may be produced if multiple branches of the regenerated giant RS axon with similar conduction velocities form synapses onto the same postsynaptic target, as has been suggested (Mackler and Selzer, 1987). Perhaps only a few small regenerated synapses—weak or strong—are needed to re-establish connections between central pattern generators above and below the lesion after the plasticity-induced changes described above occur. Additional physiological experiments on regenerated synapses of both small and giant RS axons, as well as other neuron types, will be required in order to understand exactly how regenerated synapses contribute to functional recovery.

Taken together, our data indicate that only a few small giant RS synapses are produced under conditions of functional recovery. Functional recovery is thus likely the result of a multitude of molecular and physiological changes that occur above and below the injury, including the brain, of which limited axon and synapse regeneration is only a part.

ACKNOWLEDGMENTS

Thanks to Dr. Dwight Romanowicz and the ICMB Microscopy and Imaging Facility for technical support with electron microscopy. Thanks to Dr. Ian G. Davison and Dr. Hadley W. Horch for providing helpful comments on the manuscript. This work is dedicated to R. Jason Houser, whose life inspired us to work on SCI.

LITERATURE CITED

Ahmari SE, Buchanan J, Smith SJ. 2000. Assembly of presynaptic active zones from cytoplasmic transport packets. Nat Neurosci 3:445–451.

Ayers J. 1989. Recovery of oscillator function following spinal regeneration in the sea lamprey. In: Jacklet J, editor. Cellular and neuronal oscillators. New York: Marcel Dekker. p 349–383.

Ballermann M, Fouad K. 2006. Spontaneous locomotor recovery in spinal cord injured rats is accompanied by anatomical plasticity of reticulospinal fibers. Eur J Neurosci 23: 1988–1996.

Bareyre FM, Kerschensteiner M, Raineteau O, Mettenleiter TC, Weinmann O, Schwab ME. 2004. The injured spinal cord spontaneously forms a new intraspinal circuit in adult rats. Nat Neurosci 7:269–277.

Becker CG, Lieberoth BC, Morellini F, Feldner J, Becker T, Schachner M. 2004. L1.1 is involved in spinal cord regeneration in adult zebrafish. J Neurosci 24:7837–7842.

Blesch A, Tuszynski MH. 2009. Spinal cord injury: plasticity, regeneration and the challenge of translational drug development. Trends Neurosci 32:41–47.

Bloom O, Evergren E, Tomilin N, Kjaerulff O, Low P, Brodin L, Pieribone VA, Greengard P, Shupliakov O. 2003. Colocalization of synapsin and actin during synaptic vesicle recycling. J Cell Biol 161:737–747.

Bourne J, Morgan JR, Pieribone VA. 2006. Actin polymerization regulates clathrin coat maturation during early stages of synaptic vesicle recycling at lamprey synapses. J Comp Neurol 497:600–609.

Bradbury EJ, McMahon SB. 2006. Spinal cord repair strategies: why do they work? Nat Rev Neurosci 7:644–653.

Brodin L, Shupliakov O. 2006. Giant reticulospinal synapse in lamprey: molecular links between active and periactive zones. Cell Tissue Res 326:301–310.

Brodin L, Shupliakov O, Pieribone VA, Hellgren J, Hill RH. 1994. The reticulospinal glutamate synapse in lamprey: plasticity and presynaptic variability. J Neurophysiol 72: 592–604.

Buchanan JT. 2001. Contributions of identifiable neurons and neuron classes to lamprey vertebrate neurobiology. Prog Neurobiol 63:441–466.

Buckley K, Kelly RB. 1985. Identification of a transmembrane glycoprotein specific for secretory vesicles of neural and endocrine cells. J Cell Biol 100:1284–1294.

Campos LW, Chakrabarty S, Haque R, Martin JH. 2008. Regenerating motor bridge axons refine connections and synapse on lumbar motoneurons to bypass chronic spinal cord injury. J Comp Neurol 506:838–850.

Case LC, Tessier-Lavigne M. 2005. Regeneration of the adult central nervous system. Curr Biol 15:R749–753.

Cohen AH, Mackler SA, Selzer ME. 1986. Functional regeneration following spinal transection demonstrated in the isolated spinal cord of the larval sea lamprey. Proc Natl Acad Sci U S A 83:2763–2766.

Cohen AH, Kiemel T, Pate V, Blinder J, Guan L. 1999. Temperature can alter the function outcome of spinal cord regeneration in larval lampreys. Neuroscience 90:957–965.

Cohen AH, Abdelnabi M, Guan L, Ottinger MA, Chakrabarti L. 2005. Changes in distribution of serotonin induced by spinal injury in larval lampreys: evidence from immunohistochemistry and HPLC. J Neurotrauma 22:172–188.

Cooke RM, Parker D. 2009. Locomotor recovery after spinal cord lesions in the lamprey is associated with functional and ultrastructural changes below lesion sites. J Neurotrauma 26:597–612.

Courtine G, Song B, Roy RR, Zhong H, Herrmann JE, Ao Y, Qi J, Edgerton VR, Sofroniew MV. 2008. Recovery of supraspinal control of stepping via indirect propriospinal relay connections after spinal cord injury. Nat Med 14:69–74.

Davis GR Jr, McClellan AD. 1993. Time course of anatomical regeneration of descending brainstem neurons and behavioral recovery in spinal-transected lamprey. Brain Res 602: 131–137.

Davis GR Jr, McClellan AD. 1994. Long distance axonal regeneration of identified lamprey reticulospinal neurons. Exp Neurol 127:94–105.

Davis GR Jr, Troxel MT, Kohler VJ, Grossmann EM, McClellan AD. 1993. Time course of locomotor recovery and functional

regeneration in spinal-transected lamprey: kinematics and electromyography. Exp Brain Res 97:83–95.
Deliagina TG, Zelenin PV, Fagerstedt P, Grillner S, Orlovsky GN. 2000. Activity of reticulospinal neurons during locomotion in the freely behaving lamprey. J Neurophysiol 83: 853–863.
Dubuc R, Brocard F, Antri M, Fenelon K, Gariepy JF, Smetana R, Menard A, Le Ray D, Viana Di Prisco G, Pearlstein E, Sirota MG, Derjean D, St-Pierre M, Zielinski B, Auclair F, Veilleux D. 2008. Initiation of locomotion in lampreys. Brain Res Rev 57:172–182.
Evergren E, Gad H, Walther K, Sundborger A, Tomilin N, Shupliakov O. 2007. Intersectin is a negative regulator of dynamin recruitment to the synaptic endocytic zone in the central synapse. J Neurosci 27:379–390.
Fagerstedt P, Orlovsky GN, Deliagina TG, Grillner S, Ullen F. 2001. Lateral turns in the Lamprey. II. Activity of reticulospinal neurons during the generation of fictive turns. J Neurophysiol 86:2257–2265.
Gustafsson JS, Birinyi A, Crum J, Ellisman M, Brodin L, Shupliakov O. 2002. Ultrastructural organization of lamprey reticulospinal synapses in three dimensions. J Comp Neurol 450:167–182.
Harel NY, Strittmatter SM. 2006. Can regenerating axons recapitulate developmental guidance during recovery from spinal cord injury? Nat Rev Neurosci 7:603–616.
Havton L, Kellerth JO. 1987. Regeneration by supernumerary axons with synaptic terminals in spinal motoneurons of cats. Nature 325:711–714.
Hilfiker S, Pieribone VA, Czernik AJ, Kao HT, Augustine GJ, Greengard P. 1999. Synapsins as regulators of neurotransmitter release. Philos Trans R Soc Lond B Biol Sci 354: 269–279.
Jacobs AJ, Swain GP, Snedeker JA, Pijak DS, Gladstone LJ, Selzer ME. 1997. Recovery of neurofilament expression selectively in regenerating reticulospinal neurons. J Neurosci 17:5206–5220.
Janz R, Goda Y, Geppert M, Missler M, Sudhof TC. 1999. SV2A and SV2B function as redundant Ca2+ regulators in neurotransmitter release. Neuron 24:1003–1016.
Kao HT, Porton B, Hilfiker S, Stefani G, Pieribone VA, DeSalle R, Greengard P. 1999. Molecular evolution of the synapsin gene family. J Exp Zool 285:360–377.
Kerschensteiner M, Schwab ME, Lichtman JW, Misgeld T. 2005. In vivo imaging of axonal degeneration and regeneration in the injured spinal cord. Nat Med 11:572–577.
Lichtman JW, Sanes JR. 2003. Watching the neuromuscular junction. J Neurocytol 32:767–775.
Lu P, Tuszynski MH. 2008. Growth factors and combinatorial therapies for CNS regeneration. Exp Neurol 209:313–320.
Lurie DI, Pijak DS, Selzer ME. 1994. Structure of reticulospinal axon growth cones and their cellular environment during regeneration in the lamprey spinal cord. J Comp Neurol 344:559–580.
Mackler SA, Selzer ME. 1985. Regeneration of functional synapses between individual recognizable neurons in the lamprey spinal cord. Science 229:774–776.
Mackler SA, Selzer ME. 1987. Specificity of synaptic regeneration in the spinal cord of the larval sea lamprey. J Physiol 388:183–198.
Magee JC. 2000. Dendritic integration of excitatory synaptic input. Nat Rev Neurosci 1:181–190.
Maier IC, Schwab ME. 2006. Sprouting, regeneration and circuit formation in the injured spinal cord: factors and activity. Philos Trans R Soc Lond B Biol Sci 361:1611–1634.
McClellan AD. 1994. Time course of locomotor recovery and functional regeneration in spinal cord-transected lamprey: in vitro preparations. J Neurophysiol 72:847–860.
McClellan AD, Kovalenko MO, Benes JA, Schulz DJ. 2008. Spinal cord injury induces changes in electrophysiological properties and ion channel expression of reticulospinal neurons in larval lamprey. J Neurosci 28:650–659.
Mladinic M, Muller KJ, Nicholls JG. 2009. Central nervous system regeneration: from leech to opossum. J Physiol 587: 2775–2782.
Morgan JR, Di Paolo G, Werner H, Shchedrina VA, Pypaert M, Pieribone VA, De Camilli P. 2004. A role for talin in presynaptic function. J Cell Biol 167:43–50.
Muller KJ, Scott SA. 1979. Correct axonal regeneration after target cell removal in the central nervous system of the leech. Science 206:87–89.
Murthy VN, Schikorski T, Stevens CF, Zhu Y. 2001. Inactivity produces increases in neurotransmitter release and synapse size. Neuron 32:673–682.
Nagerl UV, Kostinger G, Anderson JC, Martin KA, Bonhoeffer T. 2007. Protracted synaptogenesis after activity-dependent spinogenesis in hippocampal neurons. J Neurosci 27: 8149–8156.
Nguyen QT, Sanes JR, Lichtman JW. 2002. Pre-existing pathways promote precise projection patterns. Nat Neurosci 5: 861–867.
Ono F, Mandel G, Brehm P. 2004. Acetylcholine receptors direct rapsyn clusters to the neuromuscular synapse in zebrafish. J Neurosci 24:5475–5481.
Orlovsky GN, Deliagina TG, Wallen P. 1992. Vestibular control of swimming in lamprey. I. Responses of reticulospinal neurons to roll and pitch. Exp Brain Res 90:479–488.
Osorio J, Retaux S. 2008. The lamprey in evolutionary studies. Dev Genes Evol 218:221–235.
Photowala H, Freed R, Alford S. 2005. Location and function of vesicle clusters, active zones and Ca2+ channels in the lamprey presynaptic terminal. J Physiol 569:119–135.
Pieribone VA, Shupliakov O, Brodin L, Hilfiker-Rothenfluh S, Czernik AJ, Greengard P. 1995. Distinct pools of synaptic vesicles in neurotransmitter release. Nature 375:493–497.
Ramón y Cajal S. 1991. Cajal's degeneration and regeneration of the nervous system. DeFelipe J, Jones EG, editors. New York: Oxford University Press.
Rich MM, Wenner P. 2007. Sensing and expressing homeostatic synaptic plasticity. Trends Neurosci 30:119–125.
Richards DA, Rizzoli SO, Betz WJ. 2004. Effects of wortmannin and latrunculin A on slow endocytosis at the frog neuromuscular junction. J Physiol 557:77–91.
Rizzoli SO, Betz WJ. 2005. Synaptic vesicle pools. Nat Rev Neurosci 6:57–69.
Rovainen CM. 1967. Physiological and anatomical studies on large neurons of central nervous system of the sea lamprey (*Petromyzon marinus*). I. Muller and Mauthner cells. J Neurophysiol 30:1000–1023.
Rovainen CM. 1976. Regeneration of Muller and Mauthner axons after spinal transection in larval lampreys. J Comp Neurol 168:545–554.
Rovainen CM. 1979. Neurobiology of lampreys. Physiol Rev 59:1007–1077.
Ruff RL, McKerracher L, Selzer ME. 2008. Repair and neurorehabilitation strategies for spinal cord injury. Ann N Y Acad Sci 1142:1–20.
Sankaranarayanan S, Atluri PP, Ryan TA. 2003. Actin has a molecular scaffolding, not propulsive, role in presynaptic function. Nat Neurosci 6:127–135.
Selzer ME. 1978. Mechanisms of functional recovery and regeneration after spinal cord transection in larval sea lamprey. J Physiol 277:395–408.
Shifman MI, Zhang G, Selzer ME. 2008. Delayed death of identified reticulospinal neurons after spinal cord injury in lampreys. J Comp Neurol 510:269–282.

Shupliakov O, Bloom O, Gustafsson JS, Kjaerulff O, Low P, Tomilin N, Pieribone VA, Greengard P, Brodin L. 2002. Impaired recycling of synaptic vesicles after acute perturbation of the presynaptic actin cytoskeleton. Proc Natl Acad Sci U S A 99:14476–14481.

Son YJ, Thompson WJ. 1995. Schwann cell processes guide regeneration of peripheral axons. Neuron 14:125–132.

Spruston N. 2008. Pyramidal neurons: dendritic structure and synaptic integration. Nat Rev Neurosci 9:206–221.

Steward O, Zheng B, Tessier-Lavigne M. 2003. False resurrections: distinguishing regenerated from spared axons in the injured central nervous system. J Comp Neurol 459:1–8.

Steward O, Zheng B, Tessier-Lavigne M, Hofstadter M, Sharp K, Yee KM. 2008. Regenerative growth of corticospinal tract axons via the ventral column after spinal cord injury in mice. J Neurosci 28:6836–6847.

Takamori S, Holt M, Stenius K, Lemke EA, Gronborg M, Riedel D, Urlaub H, Schenck S, Brugger B, Ringler P, Muller SA, Rammner B, Grater F, Hub JS, De Groot BL, Mieskes G, Moriyama Y, Klingauf J, Grubmuller H, Heuser J, Wieland F, Jahn R. 2006. Molecular anatomy of a trafficking organelle. Cell 127:831–846.

Tytell ED, Lauder GV. 2004. The hydrodynamics of eel swimming: I. Wake structure. J Exp Biol 207:1825–1841.

Webb PT. 1975. Hydrodynamics and energetics of fish propulsion. Bull Fish Res Bd Can 190:1–159.

Weidner N, Ner A, Salimi N, Tuszynski MH. 2001. Spontaneous corticospinal axonal plasticity and functional recovery after adult central nervous system injury. Proc Natl Acad Sci U S A 98:3513–3518.

Wickelgren WO, Leonard JP, Grimes MJ, Clark RD. 1985. Ultrastructural correlates of transmitter release in presynaptic areas of lamprey reticulospinal axons. J Neurosci 5: 1188–1201.

Wood MR, Cohen MJ. 1979. Synaptic regeneration in identified neurons of the lamprey spinal cords. Science 206: 344–347.

Wood MR, Cohen MJ. 1981. Synaptic regeneration and glial reactions in the transected spinal cord of the lamprey. J Neurocytol 10:57–79.

Yin HS, Selzer ME. 1983. Axonal regeneration in lamprey spinal cord. J Neurosci 3:1135–1144.

Yiu G, He Z. 2006. Glial inhibition of CNS axon regeneration. Nat Rev Neurosci 7:617–627.

Zelenin PV. 2005. Activity of individual reticulospinal neurons during different forms of locomotion in the lamprey. Eur J Neurosci 22:2271–2282.

Zhang G, Jin LQ, Sul JY, Haydon PG, Selzer ME. 2005. Live imaging of regenerating lamprey spinal axons. Neurorehabil Neural Repair 19:46–57.

Ziv NE, Garner CC. 2004. Cellular and molecular mechanisms of presynaptic assembly. Nat Rev Neurosci 5:385–399.